Can simultaneous PIV in the gas and liquid phases provide insight into the transfer of momentum between the two phases?

J. H. Kim[1,*], D.B.Hann[1*], K. Johnson[1], C. N. Eastwick[1], A.V. Cherdantsev[2]
1: University of Nottingham, UK
2: Kutateladze Institute of Thermophysics, Novosibirsk, Russia
* Correspondent author: david.hann@nottingham.ac.uk

Keywords: Two phase fluids, PIV analysis, PIV technique

ABSTRACT

Understanding the interaction between a gas shearing over a liquid film and the liquid film is essential if we wish to use modeling to optimize systems to decrease environmental impact, increase efficiency and hence productivity. To this end, PIV is used to simultaneously study the velocity fields in the gas and liquid fields to better understand the interaction between the two phases.

The methodology is detailed in the paper and initial results show that the film shape changes as the flow increases from 2.2 m/s to 4.7 m/s. This change can be seen to be from a 2D surface wave regime to a 3D wave regime. In the 2D regime, the liquid film is linear in shape and the averaged and conditionally averaged velocity profiles of the gas and liquid velocity are equal at the interface.

In the 3 D regime, the averaged liquid and gas velocity profiles are no longer equal at the average interface height. Instead, they coincide at the 2.5% percentile of the local height distribution. The conditionally averaged velocity profiles show significant differences as the film height changes.

It is suggested that this would mean the use of average profiles for validating CFD in similar situations might need to be reviewed.

1. Introduction

Gas sheared flow can be observed in many engineering applications or natural phenomena. Understanding how the momentum and heat flux between these two phases are affected for different flow regimes could lead to increases in efficiency, decreases in costs and improvement in the environmental impact of a wide range of applications, such as power generation, transport, and chemical processing. In addition, this information could lead to more accurate computer models [1, 2] that could potentially be simplified using low order models to mimic complex interactions. These low order models can lead to innovative new designs that bring us a step closer to this dream.

Measuring both liquid and gas phase has been shown to provide significantly more information in the application of water waves where it has been shown [3, 4] that the roughening due to short

wave components superimposed on the longwave components can have a significant influence on the gas exchange rate in gas-liquid flows. Recently a few research works have looked at the velocity

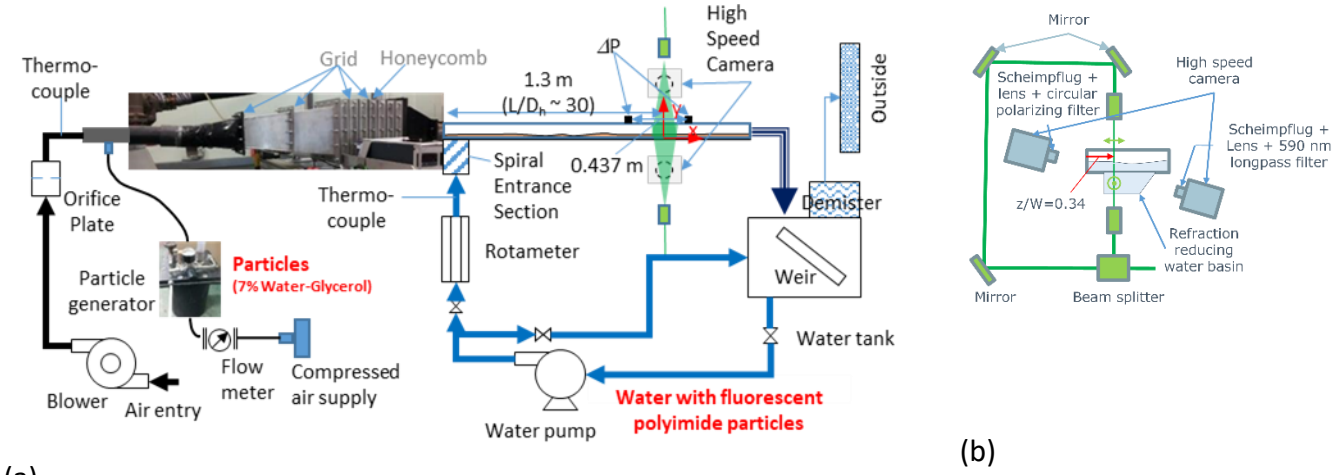

Fig 1. (a) schematic of the rig and the appratus arrangements. (b) close up on the optics to generate the dual sheet for PIV in the liquid and the gas.

field of the liquid in two phase flows in a horizontal or vertical pipe [5-7]. There are however few works looking at simultaneous measurement of thin film sheared by a gas flow[8, 9], and these have focused on gas velocities less than 2.7 m/s where the liquid phase is essentially stratified, or 2D waves. A more recent series has looked at air and liquid flow in a round pipe [10, 11], where a transition from laminar to turbulence was noted.

The work presented here is a fundamental study looking at the transition from the 2D wave regime to the 3D wave regime. These were carried out in a rectangular horizontal duct to simplify the optical access and are an extension of previous work [12]. A rectangular duct removes some issues that can occur in a circular pipe, where the thickness of the film varies with distance across the pipe. This work will hopefully lead to a better understanding of the physics occurring in higher gas velocity cases where previous work in this area has focused [13].

2. Methodology

The PIV measurements were carried out using a modified DANTEC PIV system. This system consisting of a Litron 532nm laser (LDY302-PIV) and two high-speed cameras (Phantom, v12.1). Seeding droplets for the air were generated using a Dantec 10F03 droplet generator.

The surface of the water is rough, and this can lead to variations in the light sheet intensity and location if it is only introduced from one side. To overcome this issue, the laser sheet was split into two beams. Fig 1(a) and (b) shows a schematic and the image of the arrangement of the optics, respectively. The laser light exits the light guide arm and is split by a polarizing beam splitter (Thorlabs, CM1-PBS25-532) into 2 laser beams. One of which was directed to the top-side laser sheet optic which was used to illuminate the air flow. The second beam was turned 90˚ three times

by mirrors (Thorlabs, two CM1-K13 and one CCM1-K13/M) to the bottom-side laser sheet optic to illuminate the liquid flow.

The two cameras were mounted in different ways to get optimal optical access for the measurements. 105 mm focal length lenses were used on both cameras. The upper camera that was used to measure the air flow was tilted down by 20 degree. This was because the waves on the surface blocked the view of the surface from the perpendicular view. A 3D-printed Scheimpflug adapter[1] was employed on this camera to compensate for the angle difference between the focal plane and the subject plane. There were some reflections and deflections of the lower laser light that could affect the image quality of the air-side camera, so a circular polarizing filter was attached to the lens to minimise this effect on the air-side image [10].

To seed the air, a 7% dilution ratio of glycerol-water mixture whose viscosity and surface tension are higher than those of water by 20% and 3% [14], respectively, was used. Glycerol is water-soluble liquid so that no film is formed on the interface. Moreover, the amount of the particles being considered small in comparison with the flow rate of water, the effects of the particles on the viscosity and the surface tension of the water flow will be negligible.

The lower camera viewed the water side of the two phase flow. In previous work [12] the liquid velocities were measured by viewing through the side of the film. However this work is ultimately interested in potentially sub-millimeter film thicknesses, where this is not possible. To overcome this limitation, the water side camera was tilted upwards by 40 degrees and viewed from below the

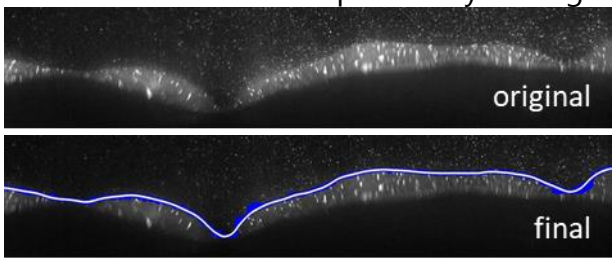

Fig 2. Example of the original image from the sideview camera and the result of the interface detection.

rig. At this angle, the light would reflect, so in order to overcome this problem, a water basin was attached to the base of the channel. The side of the basin had a 25-degree angled surface that allowed clearer viewing of the water side of the flow by reducing refraction effects.

The seeding particles for water was Rhodamine 6G-coated polyimide spherical particles with a 10 μm diameter. To help improve the detection of the interface, 0.2 g/litre of green water-colour paint was dissolved into the water but did not affect the fluid properties significantly.
To improve the image quality on the water side, a long-pass filter with cut-off wavelength of 590 nm was used to filter out the light reflected from the channel or interface and highlight only the

[1] (https://www.instructables.com/3D-Printed-Tilt-Shift-Macro-Extension-Tube/)

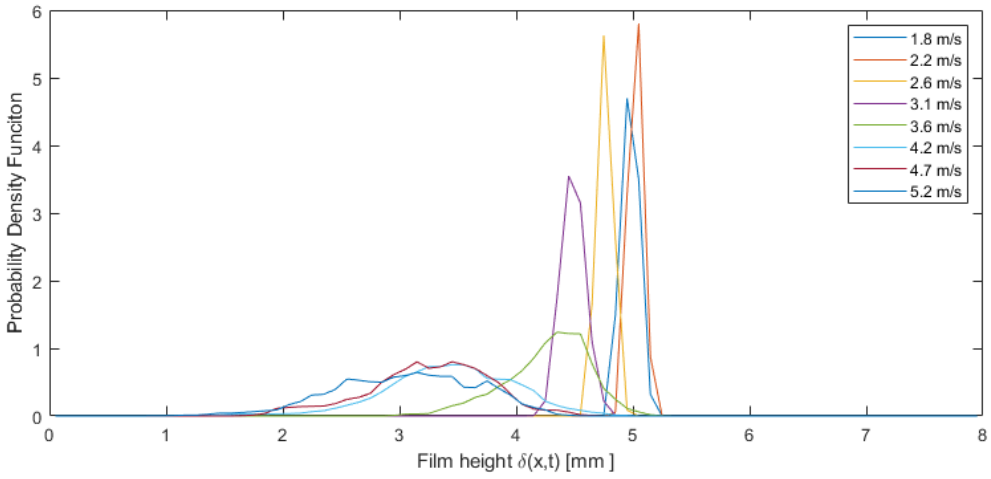

Fig 3. Probability density functions of the film height generated from the interface tracking. Note the change in width and shape to become more negatively skewed above U_{sg}=3.1 m/s

fluorescent particles. The field of view in both cameras was 24 mm wide and 15 mm high and located 1.3 m downstream from the inlet of the channel. This gave a spatial resolution of about 25 microns. The calibration target was an array of small dots on a metal plate that was placed in the plate with both a liquid film and low air flow present. This calibration plate was used to dewarp the images to account for the angling of the cameras. It also allowed the matching of the locations from both images.

After the PIV images were taken, interface detection and data conversion were made as follows. The calibration images were used to match the x-y positions in the images. The interface in an image on the air side was detected using a Matlab algorithm as shown in Fig 2. This algorithm was in several stages. Stage one removed the small particles from the images by performing a 2-dimensional median filtering with large size kernel such as 15 x 31. Then, the contrast of the image was manually adjusted to sharpen the interface in the image. A Gaussian filter with sigma = 1.1 was applied to the image and then the gradient of the image in vertical direction was calculated and another adjustment of contrast manually made. Additional algorithms are used to improve the detection in the case where the interface is blocked by the unilluminated waves closer to the camera. The interface is obtained (Fig 2) so that we can both quantify the thickness of the film and apply it as a mask to the water side images. After being de-warped based on the calibrated image data, both images were analysed to produce velocity vectors by Adaptive PIV algorithm in Dynamic Studio where the minimum interrogation area was 32 (horizontal) by 16 (vertical) with the overlap ratio of 50%.

Due to the difference between the water and gas velocity, the time separation between pairs of images had to be different. This was achieved by double pulsing the dual pulse laser with time separation of between 32 and 91 microseconds dependent on the gas velocity. The sample

frequency of these double frames was varied between 490 and 1400 Hz, dependent on the liquid velocity. Gas velocities were determined from PIV analysis between the double framed images, while liquid velocities were determined by PIV analysis between the first frames of each double frame.

The output of the experiments were detailed PIV vector maps of the gas phase at the bottom of the duct close to the liquid film and of the film, and the height of the film data in the plane of the PIV.

3. Results and discussion

Fig 3 shows the probability distribution functions of the film height. What we see is that as the gas velocity is increased, the width of the distributions increases with the region been $3.1 < U_{sg} < 3.6$ m/s being the transition region in line with [12]. The distributions display a negative skewness in

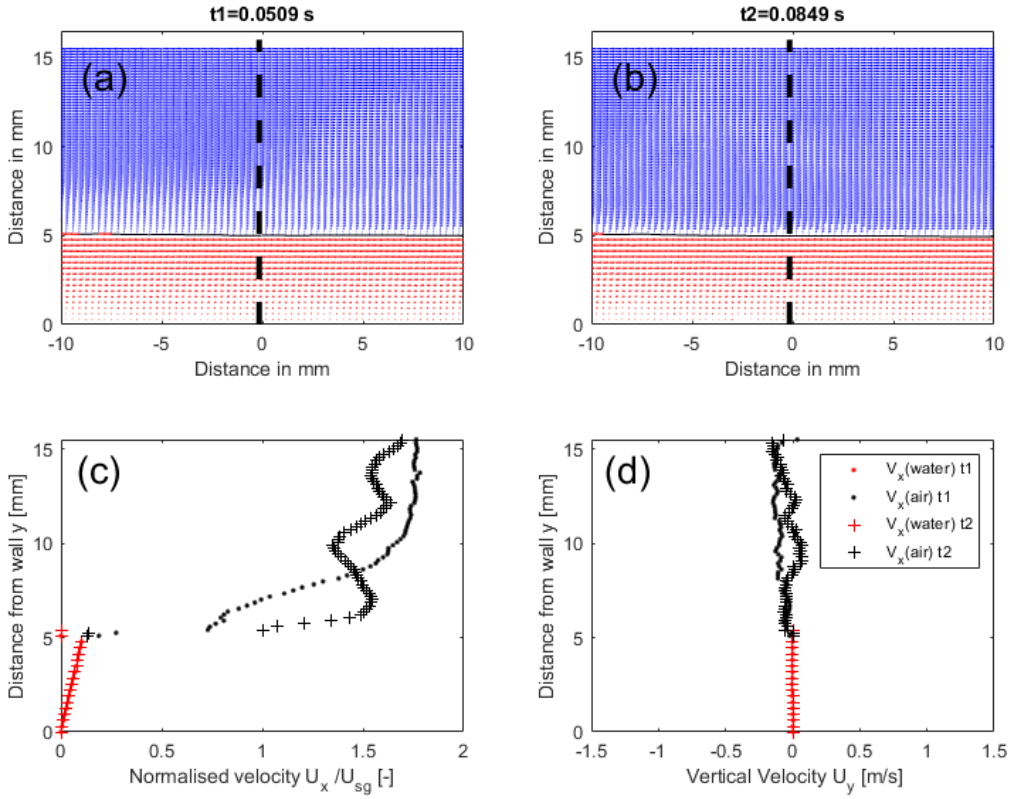

Fig 4. Sample velocity field at two time incidences chosen to demonstrate changes in velocity fields at peaks and troughs of 2D waves. (a) and (b) are two velocity fields at times showing the location of the velocity profiles, (c) shows the horizontal velocity along the profile and (d) shows the vertical velocity profile for both times. Velocity vectors in the air are scaled to make visualisation easier. $Re_L = 520$, U_{sg}=2.2 m/s

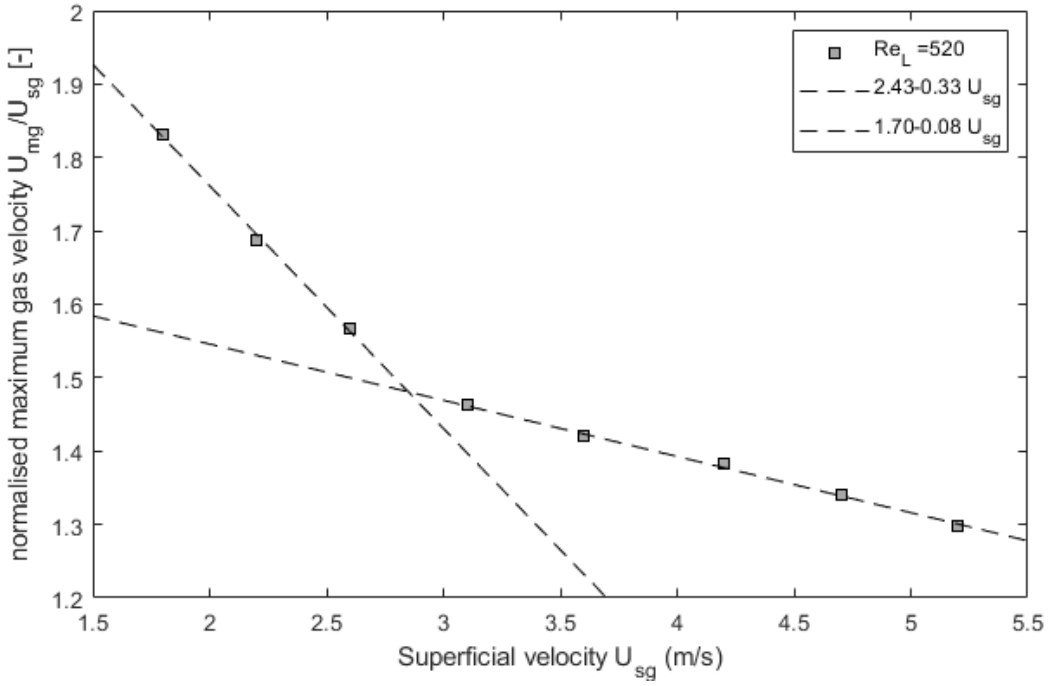

Fig 5. The ratio of maximum velocity in the gas flow divided by the superficial velocity can be seen to have a change of behaviour in the region where the liquid flow changes from the 2D to the 3D regime

the 3D regime. It is seen that in the roll wave regime ($U_{sg} > 10$ m/s) the film height distributions are positively skewed, and this change is something for further study.

Two examples of the velocity fields measured using the PIV technique at the peaks and troughs of waves in the 2D and 3D regime are shown for a liquid Reynolds number at the inlet of 520. in Fig 4 and 6 These correspond to gas superficial velocities of 2.2 m/s and 4.7 m/s and are chosen from the range of results as an example. The transition from 2D to 3D is known to occur around 3-4 m/s for this rig [12].

It is clear from Fig 4 (and Fig 3)that the wave amplitude is small for 2.2 m/s. The surface varies by of the order of 0.4 mm which is of the order of the PIV resolution. The gas velocity fluctuates significantly, and animations of the velocity fields show vortical structures being swept downstream. It should also be noted that the maximum gas velocity is of the order of 1.7 of the superficial velocity. This was also seen in Ayati et al [15] where they had the maximum velocity of the order of 1.75 of the superficial gas velocity. In line with other publications, superficial velocity is calculated using the full cross sectional area of the duct and not the gas cross-section only.

Fig 5 shows that this ratio of maximum velocity to the superficial gas velocity decreases as the superficial gas velocity is increased. There is also a sharp change in the gradient of this ratio around U_{sg} =3 m/s where the transition from 2D to 3D regime occurs as evident from Fig 3 and our previous

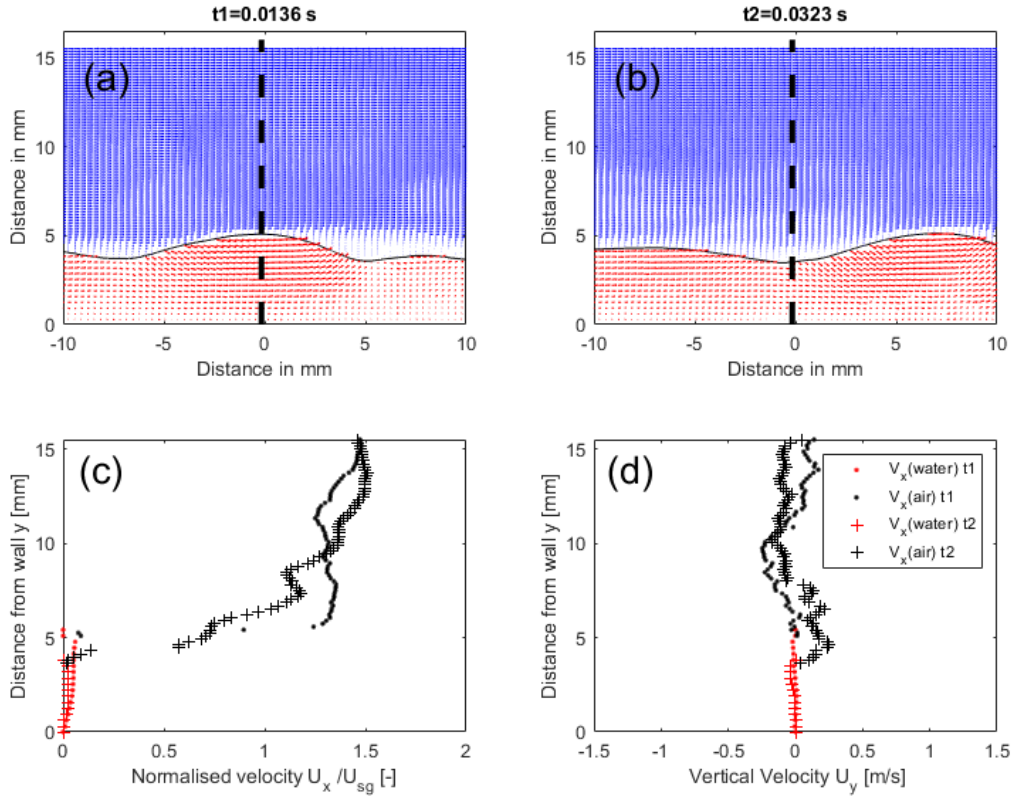

Fig 6. Sample velocity field at two incidences chosen to demonstrate changes in velocity fields at peaks and troughs of 3D waves. (a) and (b) are two velocity fields at times showing the location of the velocity profiles, (c) shows the horizontal velocity along the profile and (d) shows the vertical velocity profile for both times. Velocity vectors in the air are scaled to make visualisation easier. $Re_L = 520$, U_{sg}=4.7 m/s

work in this area [12]. This suggests that this transition has influence on the gas velocities far from the interface.

Raising the superficial gas velocity past this 2D-3D transitions, produces a clear series of 3D waves on the surface. The amplitudes of these can be seen in Fig 6. and are clearly larger than in the 2D case. Many of the features seen in the circular pipe flow of Birvaski et al [16] and the follow on work by Vollestad et al [11] are also seen here.
The gas is moving significantly faster than the liquid wave, so regions of vorticity are created in the wake of the larger waves. These regions mean that the local shear between the waves is low and has been seen to be negative in extreme cases.

It might be assumed that one can take the average of the gas velocity and liquid velocity and that they should be equal in value at the interface. This assumption is dependent on the gas and liquid flow velocities near the interface being normally distributed. In a sheared flow this is not the case because the velocity distribution will be skewed. This can be seen in the results but not shown here.

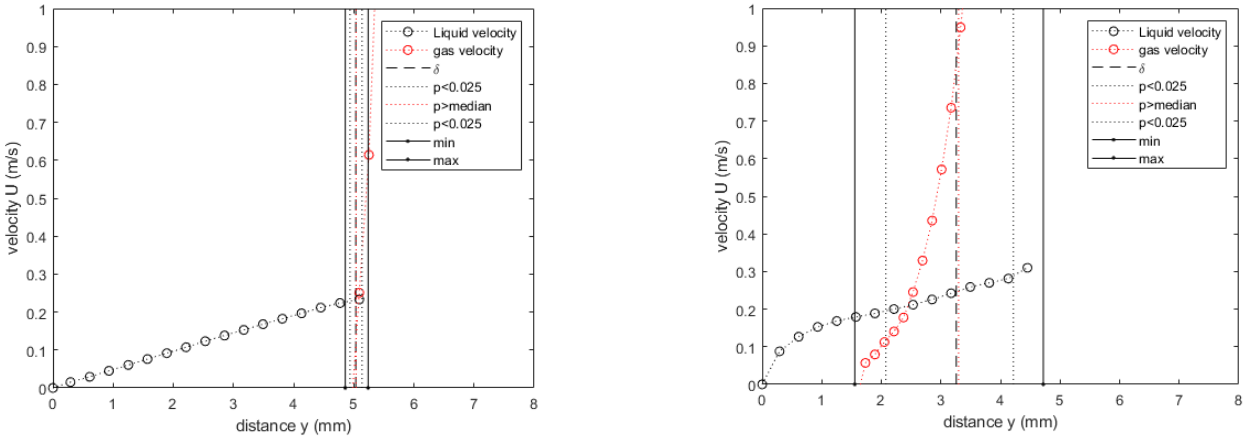

(a) $U_{sg} = 2.2\, m/s$, $Re_L = 520$ (b) $U_{sg} = 4.7\, m/s$, $Re_L = 520$

Fig 7. Average of velocity vectors in the liquid (black) and gas (red) phases only. Note that averages do not overlap at mean film thickness, but close to the 2.5% quantile for (b) and all other results in 3D regime.

In addition, the film height probability density function as shown in Fig 3 moves from normal when flow is smooth or 2D, to negatively skewed when flow becomes 3D, to positively skewed when the

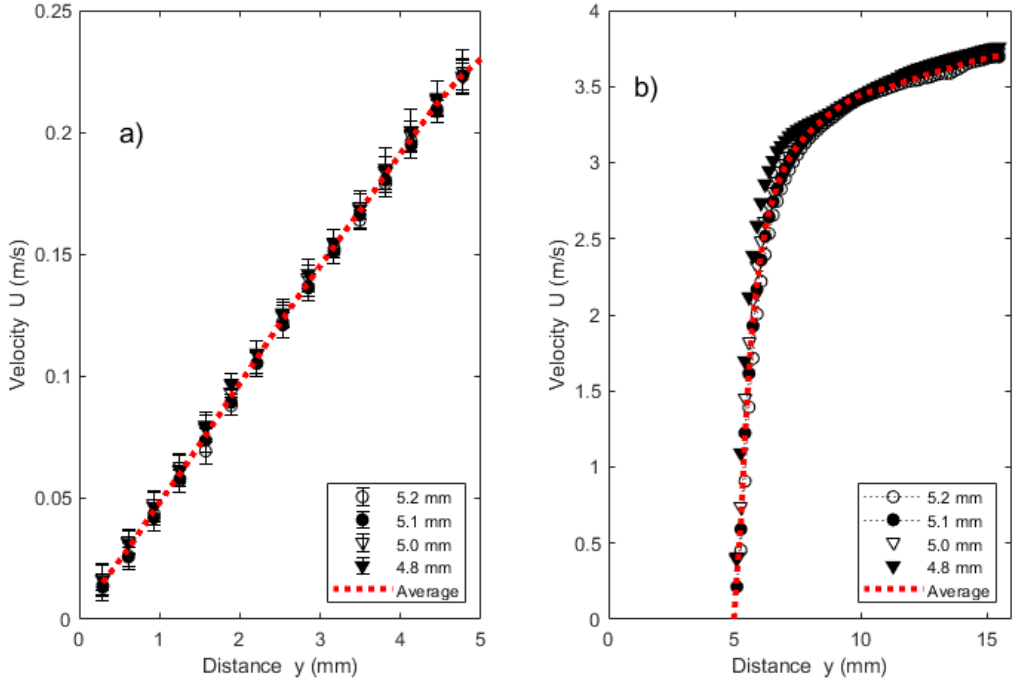

Fig 8. a) Conditional average velocity of the liquid and b) Conditional average velocity of the gas. Conditional average is done for all vector profiles with a specific film height. No significant difference can be seen. Error bars for gas velocity are not shown for clarity but are of the order of $\pm$0.75 m/s. $Re_L = 520$, U_{sg}=2.2 m/s

flow is in the roll wave regimes and above. In cases where statistics are not normal and high skewness is present, it has been suggested that it is usually inappropriate to use the mean and standard deviation [17]. This should be considered in future for results of multiphase flows where normal distributions are the exception rather than the rule.

Fig 7 (a) shows that for low gas velocity the liquid film has an average velocity profile that is linear and the average velocity of the liquid at the interface corresponds to the average velocity of the gas at the interface. However, when the gas velocity increases past the transition threshold, as shown in Fig 7 (b), this is no longer true. The average velocity of the liquid phase is now cubic in form. The gas average is biased by the vorticity regions in the wake of the liquid waves and is not linear near the interface. The steadiness of the velocity fields for $U_{sg} = 2.2\, m/s$ can be seen if we take the conditional averages. These are constructed by identifying any vertical line of PIV vectors with the same height of film, and only averaging these values. Fig 8 a) shows that the profiles of the velocity are linear for all values. For the gas flow, Fig 8 b) shows very little variation in the conditionally averaged profile. Variations are all within the fluctuations present.

For the 3D wave regime, the conditional averaged results are different. Fig 9a) demonstrates that the profile for each height is cubic in form. In this case the 2.1 mm conditionally averaged velocity rises slightly close to the liquid surface, but examples of decrease have been seen in individual cases. This would suggest that negative flow of the gas in the wake of a wave can slow the liquid surface below it.

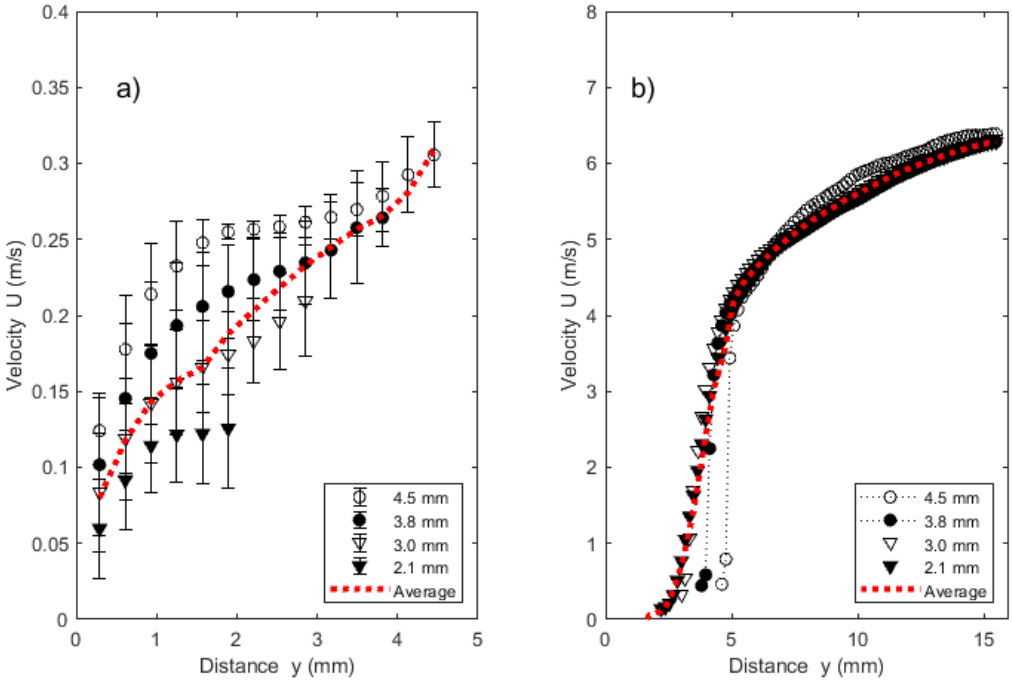

Fig 9. a) Conditional average velocity of the liquid and b) Conditional average velocity of the gas. Conditional average is done for all vector profiles with a specific film height. Significant differences can be seen. Error bars for gas velocity are not shown for clarity but are of the order of $\pm$0.75 m/s. $Re_L = 520$, U_{sg}=4.7 m/s

The conditional averaged gas profiles are shown in Fig 9 b). As evident in the earlier velocity vector maps (Fig 6 (c)), the interfacial shear above the surface when the wave crest passes is more intense. The average of the gas velocity is closer to the profiles for the conditional average when the film is lower. This is not unexpected due to the negative skewness noted previously.
This has implications when these types of flows are modelled in CFD. Further work is being carried out to use this data as validation for models being generated as part of this project.

4. Conclusions

In this paper, the velocity fields in both the gas and liquid phase were measured simultaneously as well as the film height. The focus of this work was to identify differences in the gas and liquid flows as the gas velocity is increased and the flow regime changes from the 2D wave to the 3D wave regime.
It was noted that the film height probability function transitions from a normal distribution in the 2D regime to a negatively skewed one in the 3D regime.
In the 2D regime, the velocity in the liquid phase increases linearly with height and the velocities of the liquid and the gas correspond to each other at the interface. Vortical structures are seen in the gas flow, but the averages suggest that these are due to the surface being mildly rough. In the 3D regime this is no longer true. The averaged and conditionally averaged velocity profiles show a cubic shape for the liquid phase. In the gas phase, the velocity profile above a crest produces significantly more shear on the liquid than between the crests. In both phases for the 3D case, the "averaged" profiles of the velocity do not appear to be appropriate to describe the statistics. Further understanding of the statistics might prove useful for comparison of data with CFD generated results.

Acknowledgements

Dr Hann thanks Rolls-Royce plc and the EPSRC for the support under the Prosperity Partnership Grant Cornerstone: Mechanical Engineering Science to Enable Aero Propulsion Futures, Grant Ref: EP/R004951/1

References

[1] A. A. Adeniyi, "A coupled Lagrangian-Eulerian framework to model droplet to film interaction with heat transfer," Ph.D., University of Nottingham, 2015.

[2] A. A. Hashmi, *Oil film dynamics in aero engine bearing chambers : fundamental investigations and numerical modelling*. Berlin: Logos, 2012.

[3] E. J. Bock, T. Hara, N. M. Frew, and W. R. McGillis, "Relationship between air-sea gas transfer and short wind waves," *Journal of Geophysical Research: Oceans,* Article vol. 104, no. C11, pp. 25821-25831, 1999, Art no. 1999jc900200.

[4] S. Longo, "Wind-generated water waves in a wind tunnel: Free surface statistics, wind friction and mean air flow properties," *Coastal Engineering,* Article vol. 61, no. 1, pp. 27-41, 2012, doi: 10.1016/j.coastaleng.2011.11.008.

[5] M. Birvalski, M. J. Tummers, R. Delfos, and R. A. W. M. Henkes, "PIV measurements of waves and turbulence in stratified horizontal two-phase pipe flow," *Int. J. Multiph. Flow,* Article vol. 62, pp. 161-173, 2014, doi: 10.1016/j.ijmultiphaseflow.2014.03.001.

[6] I. Zadrazil and C. N. Markides, "An experimental characterization of liquid films in downwards co-current gas-liquid annular flow by particle image and tracking velocimetry," *Int. J. Multiph. Flow,* Article vol. 67, no. S, pp. 42-53, 2014, doi: 10.1016/j.ijmultiphaseflow.2014.08.007.

[7] A. C. Ashwood *et al.*, "A multiphase, micro-scale PIV measurement technique for liquid film velocity measurements in annular two-phase flow," *Int. J. Multiph. Flow,* vol. 68, pp. 27-39, 2015, doi: 10.1016/j.ijmultiphaseflow.2014.09.003.

[8] M. A. André and P. M. Bardet, "Interfacial shear stress measurement using high spatial resolution multiphase PIV," *Experiments in Fluids,* vol. 56, no. 6, 2015, Art no. 132, doi: 10.1007/s00348-015-2006-7.

[9] M. A. André and P. M. Bardet, "Velocity field, surface profile and curvature resolution of steep and short free-surface waves," *Experiments in Fluids,* vol. 55, no. 4, 2014, Art no. 1709, doi: 10.1007/s00348-014-1709-5.

[10] M. Birvalski, M. J. Tummers, and R. A. W. M. Henkes, "Measurements of gravity and gravity-capillary waves in horizontal gas-liquid pipe flow using PIV in both phases," *Int. J. Multiph. Flow,* Article vol. 87, pp. 102-113, 2016, doi: 10.1016/j.ijmultiphaseflow.2016.09.003.

[11] P. Vollestad, A. A. Ayati, L. Angheluta, J. H. LaCasce, and A. Jensen, "Experimental investigation of airflow above waves in a horizontal pipe," *Int. J. Multiph. Flow,* Article vol. 110, pp. 37-49, 2019, doi: 10.1016/j.ijmultiphaseflow.2018.08.008.

[12] D. B. Hann, Loizou, Katerina, Vasques, Joao, C., Tokarev, Mikhail.P, Cherdantsev, Andrey. V, "The use of POD filtering to study the transition from 2D to 3D in stratified two-phase flow," presented at the 19th International Symposium on the Application of Laser and Imaging Techniques to Fluid Mechanics, Lisbon Portugal, JULY 16 – 19, 2018.

[13] A. V. Cherdantsev, D. B. Hann, and B. J. Azzopardi, "Study of gas-sheared liquid film in horizontal rectangular duct using high-speed LIF technique: Three-dimensional wavy structure and its relation to liquid entrainment," *International Journal of Multiphase Flow,* vol. 67, pp. 52-64, 2014, doi: 10.1016/j.ijmultiphaseflow.2014.08.003.

[14] S. Mallinson, G. McBain, and G. Horrocks, "Viscosity and surface tension of aqueous mixtures," in *20th Australasian Fluid Mechanics Conference Perth, Australia. Australasian Fluid Mechanics Society*, 2016.

[15] A. A. Ayati, J. Kolaas, A. Jensen, and G. W. Johnson, "Combined simultaneous two-phase PIV and interface elevation measurements in stratified gas/liquid pipe flow," *International Journal of Multiphase Flow,* Article vol. 74, pp. 45-58, 2015, doi: 10.1016/j.ijmultiphaseflow.2015.03.024.

[16] M. Birvalski, M. J. Tummers, R. Delfos, and R. A. W. M. Henkes, "Laminar-turbulent transition and wave-turbulence interaction in stratified horizontal two-phase pipe flow," *Journal of Fluid Mechanics,* Article vol. 780, pp. 439-456, 2015, doi: 10.1017/jfm.2015.483.

[17] A. L. Bowley, *Elements of Statistics* (no. v. 2). P.S. King, 1920.